THE JOURNAL OF PHYSICAL CHEMISTRY C

ARTICLE

pubs.acs.org/JPCC

Low-Energy Electron-Induced Decomposition and Reactions of Adsorbed Tetrakis(trifluorophosphine)platinum [$Pt(PF_3)_4$]

Kees Landheer,[†] Samantha G. Rosenberg,[‡] Laurent Bernau,[§] Petra Swiderek,[||] Ivo Utke,[§] Cornelis W. Hagen,[†] and D. Howard Fairbrother*,[‡]

[†]Faculty of Applied Sciences, Delft University of Technology, Lorentzweg 1, 2628CJ Delft, The Netherlands

[‡]Department of Chemistry, Johns Hopkins University, Baltimore, Maryland 21218, United States

[§]Swiss Federal Laboratories for Materials Science and Technology, EMPA, Feuerwerkerstrasse 39, 3602 Thun, Switzerland

[||]Institute of Applied and Physical Chemistry, Fachbereich 2 (Chemie/Biologie), Universität Bremen, 28334 Bremen, Germany

S Supporting Information

ABSTRACT: The effect of ~500 eV electrons on nanometer-thick films of the platinum precursor tetrakis(trifluorophosphine)platinum [$Pt(PF_3)_4$] has been studied in situ under ultra-high-vacuum (UHV) conditions using a combination of X-ray photoelectron spectroscopy (XPS), mass spectrometry (MS), and high-resolution electron energy loss spectroscopy (HREELS). Electron irradiation of adsorbed $Pt(PF_3)_4$ molecules initially proceeds through a single Pt—P bond-cleavage event and the ejection of one PF_3 ligand, analogous to the electron-stimulated reactions of $Pt(PF_3)_4$ in the gas phase. The electron-stimulated deposition cross section of $Pt(PF_3)_4$, $\sigma_{Pt(PF_3)_4}$, is governed by the rate of this initial Pt—PF_3 cleavage event, which is calculated to be ~2.5×10^{-15} cm^2 at an incident electron energy of 500 eV. In contrast to the initial deposition step, subsequent electron-stimulated reactions of the surface-bound $Pt(PF_3)_3$ intermediate occur exclusively through P—F bond cleavage and the release of fluorine into the gas phase. In this second phase of the decomposition process, oxygen uptake into the film is observed because of reactions between water vapor and the coordinatively unsaturated phosphorus atoms formed by P—F bond cleavage. Electron-beam-induced deposition (EBID) of $Pt(PF_3)_4$ was also performed by electron irradiating a substrate at room temperature and at higher electron fluxes, in the presence of a constant partial pressure of $Pt(PF_3)_4$. The absence of fluorine in these films underscores the role of electron-stimulated P—F bond cleavage, whereas the absence of oxygen highlights the important role that deposition conditions (e.g., substrate temperature and background gas composition) play in determining the ultimate composition of typical EBID films.

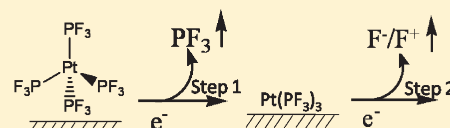

I. INTRODUCTION

Electron-beam-induced deposition (EBID), also referred to as focused electron-beam-induced processing (FEBIP), is a low-vacuum materials processing technique in which a focused electron beam is used to directly write nanometer-sized structures onto a substrate in a constant partial pressure of precursor molecules.[1−4] EBID has a unique and attractive combination of capabilities, including high spatial resolution and the flexibility to deposit self-supporting three-dimensional nanostructures on nonplanar surfaces. EBID offers a number of advantages compared to other vacuum-based nanofabrication strategies. EBID is capable of creating smaller features than ion-beam-induced deposition (IBID), with less amorphization and without ion implantation.[5−7] Although the resolution of EBID is comparable to that of electron beam lithography (EBL) and extreme ultraviolet lithography (EUVL),[8,9] it needs no resist layers or etching step for pattern transfer. The advantages of EBID have also been recently been combined with those of atomic layer deposition (ALD) to create purely metallic but geometrically well-defined nanostructures.[10] Current applications of EBID include repairing masks used in UV lithography,[11−14] creating line gratings on vertical cavity surface emitting lasers,[15] and fabricating tips for scanning probe microscopy.[16,17]

Perhaps the most important class of EBID materials, with potential applications ranging from nanowires to biosensors, is that of metallic nanostructures created from volatile organometallic precursors.[18−20] Within this category, platinum-containing EBID precursors are among the most widely used, particularly trimethyl(methylcyclopentadienyl) platinum(IV) ($MeCpPtMe_3$), which has been used to create nanowires and local contact points for carbon nanotubes.[21−23] However, one of the limitations of deposits grown using $MeCpPtMe_3$ is the often unacceptably high degree of carbon contamination, which negatively impacts conductivity.[24−27] In an attempt to overcome the deleterious effects of carbon contamination, a number of deposition experiments have been performed using the carbon-free EBID platinum precursor tetrakis(trifluorophosphine)platinum [$Pt(PF_3)_4$].[28−30] This high-vapor-pressure liquid (68 Torr at 20 °C)[31] has already been used in chemical vapor deposition (CVD) to create pure platinum films on a variety of heated (200−300 °C) substrates[32] and in selective-area deposition of platinum silicide on Si(100).[33] $Pt(PF_3)_4$ has also been used in UV-laser-induced metallization

Received: May 5, 2011
Revised: July 17, 2011
Published: July 20, 2011

 © 2011 American Chemical Society

studies, where deposition has been ascribed to dissociative electron capture involving low-energy electrons produced by laser−surface interactions.[34] A comparison of EBID structures generated from $Pt(PF_3)_4$ and $MeCpPtMe_3$ reveals the advantages of using $Pt(PF_3)_4$. The resistivity measured for a line deposit created from $MeCpPtMe_3$ by 20 keV electrons at a beam current of 2.4 nA was $1.5 \times 10^3\ \mu\Omega$ cm,[30] whereas that of a comparable line created from the $Pt(PF_3)_4$ precursor using 10 keV electrons at a beam current of 2.8 nA was 641 $\mu\Omega$ cm.[28] The lowest resistivity achieved for a line deposit of $Pt(PF_3)_4$ is 26 $\mu\Omega$ cm created with a beam current of 13 nA,[28] a value only 2.5 times greater than that of pure platinum (10.42 $\mu\Omega$ cm) and orders of magnitude lower than the resistivity of EBID nanowires created with $MeCpPtMe_3$.

Despite the advantages of using $Pt(PF_3)_4$, a detailed understanding of how the ultimate chemical composition and crystallinity of deposits are influenced by the deposition conditions remains largely elusive. Indeed, this highlights the lack of knowledge regarding the chemical reactions and transformations that underpin EBID. Nanostructures created from $Pt(PF_3)_4$ often contain significant concentrations of residual phosphorus[28−30] and oxygen,[29,30] whose presence will adversely impact many desirable materials properties such as catalytic activity. To improve film composition, various deposition and postdeposition approaches have been developed to increase the platinum content of $Pt(PF_3)_4$ deposits. For example, Wang et al. showed that the Pt concentration increases when deposition occurs in the presence of O_2 and when substrate temperatures above room temperature are used during deposition.[29] Postdeposition electron beam irradiation and annealing also improve the Pt content, crystallinity, and conductivity of EBID structures created from $Pt(PF_3)_4$.[35,36] Takeguchi et al. also reported that, by combining postdeposition electron beam irradiation with 300 keV electrons and in situ annealing at about 130 °C, the phosphorus concentration can be reduced.[37]

To develop a more detailed, atomistic understanding of EBID, the present study focuses on identifying the reaction steps and chemical transformations that accompany the electron-induced decomposition of adsorbed $Pt(PF_3)_4$ molecules. In terms of improving the ability to rationalize how the deposition processes influence the ultimate composition of EBID materials, understanding the electron-stimulated reactions of adsorbed precursor molecules can be viewed as a necessary first step, as the initial event in EBID must involve an electron-stimulated dissociation event. Consequently, the electron-induced reactions of adsorbed precursors will always influence the film's ultimate composition.

In typical EBID experiments performed in electron microscopes or auger electron spectrometers, nanostructures are created by irradiating a substrate with a focused electron beam in the presence of a constant partial pressure of precursor molecules.[1−3] Deposition is typically performed at ambient substrate temperatures; consequently, there is no chemisorption of intact precursor molecules when the gas flow is turned off, and both thermal and electron-stimulated reactions can be operational. To reduce the complexity of the deposition process and isolate the elementary surface reactions and reaction cross sections that contribute solely to the electron-induced decomposition of adsorbed precursor molecules such as $Pt(PF_3)_4$, we have adopted an ultra-high-vacuum (UHV) surface science approach, in which nanoscale thin films of precursor molecules have been adsorbed onto solid substrates at low temperatures (∼160 K).[38−41] In these studies, we have used low-energy (∼500 eV) flood guns to generate a relatively broad and defocused electron beam that exhibits a roughly uniform flux over an area comparable to the size of the substrate (∼1 cm^2). This experimental approach then allows for the application of traditional surface analytical techniques to study the electron-stimulated surface reactions. Although the energy of the incident electrons (500 eV) is less than the higher energies (typically >5 keV) used to create EBID structures in electron microscopes, this is less of a disconnect than it might appear to be, as it is widely recognized that the low-energy secondary electrons generated by the interaction of the comparatively high-energy primary beam with the substrate make a significant contribution to the EBID process.[42] In the present investigation, the effects of electron beam irradiation on the adlayer have been monitored in situ using X-ray photoelectron spectroscopy (XPS), mass spectrometry (MS), and high-resolution energy loss spectroscopy (HREELS). Comparable studies have been performed on the electron-induced surface reactions of several EBID precursors such as hexafluoracetylacetonate copper(I) vinyltrimethylsilane,[43] metal carbonyls,[44−47] and more recently $Au^{III}(acac)Me_2$[38] and $MeCpPtMe_3$.[39] UHV surface science studies have also proved effective in studying other electron-mediated processes, including chemical and physical transformations initiated in organic thin films.[48−53]

In the context of EBID, the UHV environment has several important advantages that facilitate a more detailed understanding of the electron-stimulated reactions involved in deposition and precursor decomposition.[41] For example, the absence of a constant partial pressure of precursor molecules facilitates the detection and identification of volatile gas-phase species that might be produced during the electron beam irradiation of organometallic precursors, and any unwanted effects of contaminant gases are circumvented.[39−41] In addition, the use of comparatively low substrate temperatures means that electron-stimulated processes can be isolated in the absence of any thermal reactions and effects (e.g., diffusion). An additional and specific advantage of $Pt(PF_3)_4$ is that, in contrast to other EBID precursors, it does not contain hydrogen, an element that cannot be detected using electron-based spectroscopies. Consequently, XPS could monitor and quantify the coverage of all of the three elements present in the $Pt(PF_3)_4$ precursor during electron irradiation; this proved extremely useful in this work and allowed for the identification of the two sequential steps that collectively describe the electron-stimulated reactions of adsorbed $Pt(PF_3)_4$. To provide a point of comparison to more typical EBID experiments, we also created a film on a substrate at room temperature in an Auger electron spectrometer, using a focused electron beam to initiate deposition in the presence of a constant partial pressure of $Pt(PF_3)_4$.

II. EXPERIMENTAL SECTION

A. UHV Studies. The majority of the experiments in this investigation probed, in situ ($P_{base} < 5 \times 10^{-9}$ Torr), the effect of low-energy broad-beam electron irradiation on nanometer-thick films of tetrakis(trifluorophosphine)platinum [$Pt(PF_3)_4$] deposited at low temperatures (<165 K) onto solid substrates under UHV conditions. At Johns Hopkins University (JHU), the effects of electron irradiation on $Pt(PF_3)_4$ were probed by X-ray photoelectron spectroscopy (XPS) and mass spectrometry (MS),[38,39] and at Universität Bremen, they were probed by high-resolution electron energy loss spectroscopy (HREELS).[54]

Precursor. Tetrakis(trifluorophosphine)platinum (CAS 19529-53-4, Strem Chemicals, Inc.) [$Pt(PF_3)_4$] is a tetrahedral organometallic

complex that exists as a high-vapor-pressure liquid (68 Torr at 20 °C) at standard temperature and pressure (STP).[31] At JHU, the precursor was stored in a cooled stainless steel cylinder, whereas at Bremen, the $Pt(PF_3)_4$ was stored in a glass tube held at 4 °C. In both setups, the $Pt(PF_3)_4$ was attached to an external gas dosing line and purified by a freeze−pump−thaw cycle to remove any residual PF_3 gas prior to dosing.

Surface Science Studies. The effects of electron irradiation on adsorbed $Pt(PF_3)_4$ molecules were studied in two UHV chambers, one at JHU and one at Bremen. At JHU, substrates were mounted onto dedicated manipulators with capabilities for *xyz* translation and rotation, as well as sample cooling and heating. Sample temperatures were measured with a thermocouple attached directly to the substrate. At Bremen, samples were mounted onto the tip of a closed-cycle helium cryostat attached to a bellows, allowing for *z* travel into the HREELS chamber. The HREEL spectrometer can also be moved in the horizontal direction perpendicular to the *z* direction, thereby providing limited translation in the *x* direction. A limited tilt could be achieved by means of a short bellows with three adjustable screws mounted between the cryostat and the *z* bellows. Sample temperature was measured with a Si diode mounted into the Cu block onto which a sapphire window carrying the Pt foil was press fit.

Substrates. For XPS and MS experiments at JHU, an amorphous carbon (a-C) substrate was used as an inert surrogate. Because the precursor lacked any carbon atoms, this allowed XPS to monitor and quantify changes in the chemical composition of the adlayer. Atomically clean a-C substrates were generated by sputtering a 1.5 cm^2 highly oriented pyrolytic graphite (HOPG) substrate (SPI Supplies) with 4 keV Ar^+ (>1 h). At Bremen, the substrate for the HREELS investigations was a polycrystalline Pt foil with a surface area of 3.8 cm^2. Prior to each deposition, the substrate was cleaned by high-temperature resistive heating of the Pt foil for 2−5 s in vacuo.

Creating $Pt(PF_3)_4$ Films. In most experiments at JHU, a submonolayer-thick $Pt(PF_3)_4$ film was created by dosing the precursor onto the substrate at an uncorrected pressure reading of 1×10^{-7} Torr as measured by the ion gauge, for about 60 s. During dosing and subsequent electron irradiation, the substrate was cooled to ∼160 K. In these experiments, the average $Pt(PF_3)_4$ coverage was determined by measuring the attenuation of the C 1s XPS peak area associated with the HOPG substrate after dosing, assuming an inelastic mean free path of 2 nm for C 1s photoelectrons.[55] Data from experiments (Figure S1, Supporting Information) in which the thickness of the adlayer was measured as a function of the $Pt(PF_3)_4$ exposure indicated that a 6 Langmuir dose (1 Langmuir corresponds to an exposure of 1×10^{-6} Torr for 1 s) creates a film thickness of ∼0.12 nm. Based on the volume occupied by one $Pt(PF_3)_4$ molecule determined from X-ray crystallography[56] and the assumption that $Pt(PF_3)_4$ uniformly wets the surface, a film thickness of ∼0.12 nm corresponds to a coverage of ∼0.16 ML. In this definition, 1 ML refers to the coverage of $Pt(PF_3)_4$ molecules (assuming uniform wetting) that would be required to produce a film thickness equal to the effective diameter of the $Pt(PF_3)_4$ molecule (assuming a spherical shape).

In HREELS experiments, a $Pt(PF_3)_4$ film was created by dosing the precursor onto a Pt substrate cooled to ∼20−30 K. The precursor was leaked into the dosing chamber from a calibrated volume, and the exposure was estimated by measuring the pressure decrease within the gas dosing line. Monolayer

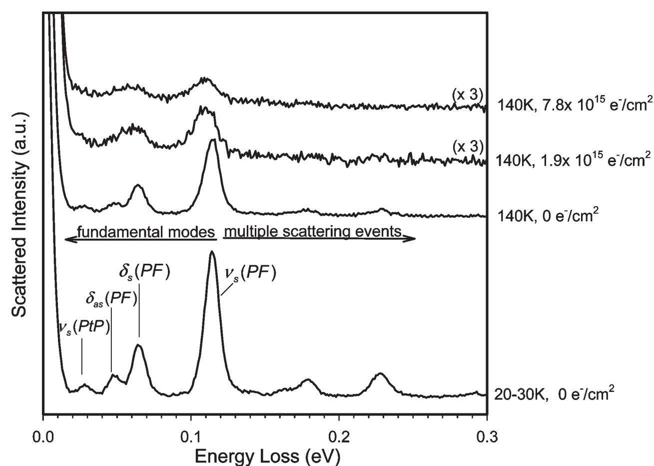

Figure 1. HREEL spectrum of ∼3 ML of $Pt(PF_3)_4$ adsorbed onto a polycrystalline Pt foil at 20−30 K (bottom spectrum). HREEL spectra at the top show the changes that occur when the $Pt(PF_3)_4$ adlayer is annealed to 140 K and then exposed to 500 eV electrons.

$Pt(PF_3)_4$ coverages were estimated from HREELS data, based on the appearance of multiple scattering bands (see Figure 1). These features correspond to loss peaks caused by electrons that have undergone multiple inelastic scattering events with different adsorbed molecules.[57] Because the $Pt(PF_3)_4$ was dosed from a calibrated volume, once the exposure that corresponded to a monolayer was deduced, subsequent coverages could be determined directly from the exposure. In practice, a film thickness corresponding to ∼3 ML was created by dosing $Pt(PF_3)_4$ until a pressure drop of 1 μbar was observed in the gas dosing line.

Electron Source. For all experiments at JHU and Bremen, a commercial flood gun (Specs FG 15/40) was used as the source of broad-beam electron irradiation. For experiments performed at JHU, the flood gun was positioned perpendicular to the substrate at a sample−source distance of ∼12 cm. The electron beam profile had previously been characterized using a Faraday cup attached to the UHV manipulator;[40] data from these studies showed that, by positioning the sample at the center of the beam profile and at a source-to-sample distance greater than 7 cm, a relatively uniform electron flux across the surface (∼10% change across a 2.0 cm^2 substrate) could be obtained. The incident electron energy was calculated from the sum of the electron energy generated by the flood gun (480 eV) and a positive bias (typically +20 V) applied to the substrate to ensure that the vast majority of the secondary electrons generated by the primary beam did not escape into vacuum. Unless noted, the applied target current was 5 μA.

For the HREELS experiments, the flood gun was mounted at 60° with respect to the sample normal, and no positive bias was applied to the sample during irradiation. The current on the sample during electron exposure was 60−80 μA (∼15−20 μA/cm^2) for an electron energy of 500 eV.

For all of the experiments, electron irradiation is reported in terms of the electron dose (D), determined using the equation

$$D = \frac{It}{A} \qquad (1)$$

where I is the measured target current (in electrons per second), t is the duration of electron exposure (in seconds), and A is the sample area (in square centimeters). At JHU and Bremen, a

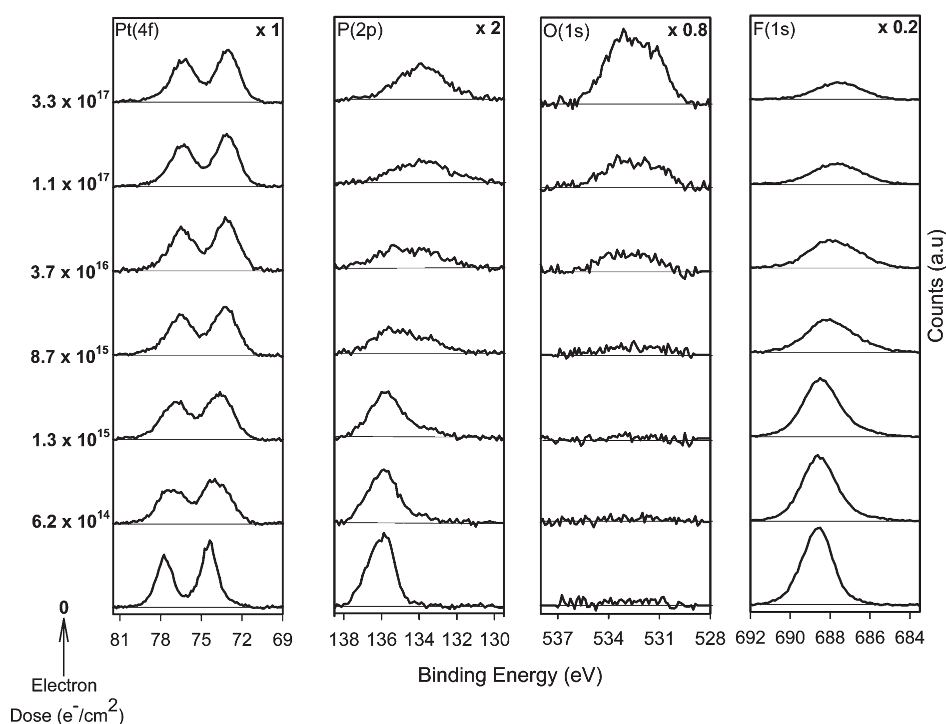

Figure 2. Effects of electron irradiation (500 eV electrons; constant target current of 5 μA) on the Pt 4f, P 2p, O 1s, and F 1s XPS regions of $Pt(PF_3)_4$ (submonolayer coverages) adsorbed onto an amorphous carbon substrate. The raw XPS data were adjusted using a Shirley background subtraction. To maximize resolution of XPS peak shapes, spectra were acquired at a pass energy of 22 eV.

picoammeter connected to the substrate was used to monitor the target current.

Analytical Techniques. X-ray Photoelectron Spectroscopy. XPS was performed with a Physical Electronics 5400 system using Mg Kα X-rays ($h\upsilon$ = 1253.6 eV). All XP spectra were deconvoluted using commercially available software (CASA XPS), and all peak positions were aligned to the C 1s peak of HOPG at 284.5 eV.[58] XP spectra were measured with a step size of 0.125 eV and at pass energies of either 89 or 22 eV. XPS experiments at 89 eV pass energy were used to determine fractional coverages, whereas separate experiments at 22 eV pass energy focused on measuring changes in the XPS peak shapes and shifts in binding energies that occurred as a result of electron irradiation.

In control experiments, the effect of X-ray irradiation alone on $Pt(PF_3)_4$ adlayers was evaluated. Results from these studies, shown in the Supporting Information (Figure S2), indicate that prolonged X-ray irradiation produces qualitatively similar changes to the spectral envelopes and fractional surface coverages as observed for very low total electron doses from the flood gun, where the latter is shown in Figures 2 and 3. The effects of X-ray irradiation include a small (~10%) loss of the nascent phosphorus and fluorine atoms at similar rates, such that the ratio of phosphorus to fluorine atoms remains the same as in the parent molecule. It should be noted that, in these control studies, a very small signal was observed in the O 1s region, presumably a result of water adsorption, although the oxygen signal intensity remained constant throughout the period of X-ray irradiation (see Figure S2, Supporting Information). The similarity in the effects of electron (Figures 2 and 3) and X-ray (Figure S2, Supporting Information) bombardment is almost certainly a consequence of X-ray-induced transformations being initiated by low-energy secondary electrons generated by X-ray interactions with the substrate and the adsorbed $Pt(PF_3)_4$ molecules. As noted, the compositional changes induced by X-ray irradiation occurred at a much lower rate compared to the effects of electrons generated by the flood gun. Thus, a comparison of Figure S2 (Supporting Information) and Figure 3 reveals that 108 min of X-ray irradiation, the scan time necessary to complete approximately six full scans of the Pt 4f, O 1s, F 1s, and P 2p regions, produced roughly the same changes to the adlayer as an electron dose of $\sim 2 \times 10^{14}$ e^-/cm^2 for 500 eV electrons. Consequently, all of the changes in the Pt 4f, O 1s, F 1s, and P 2p regions observed in Figures 2−4 by XPS are dominated (>95%) by the effects of the electrons generated by the flood gun.

Mass Spectrometry. A quadrupole mass spectrometer was used to monitor neutral gas-phase products that evolved during electron irradiation. The spectrometer (Stanford Research System, 0−200 amu) was positioned ~10 cm from the substrate and in a direct line-of-sight. During dosing, the spectrometer was also used to routinely check the purity of the $Pt(PF_3)_4$.

High-Resolution Electron Energy Loss Spectroscopy. The Ibach-type HREELS instrument consisted of a double-pass monochromator and a single-pass analyzer, with cylindrical deflectors as energy-dispersing elements. Scattered electrons were collected at the specular angle (60°) of detection with respect to the surface normal. The energy of the primary beam used to acquire HREELS data was 5.5 eV. The incident energy was calibrated to within ±0.2 eV using the onset of the transmitted current and further corrected for cutoff effects from the lenses by putting a retarding field on the target.[59] The spectrometer was operated with a resolution of about 10 meV, as measured by the full width at half-maximum (fwhm) of the elastic peak, for currents transmitted through the sample on the

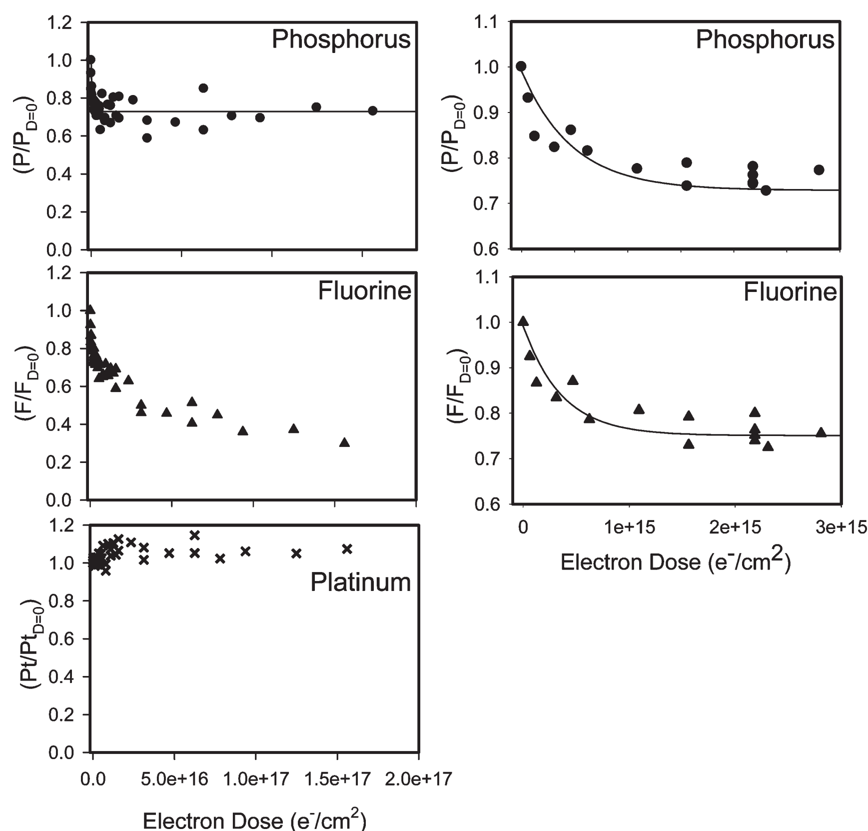

Figure 3. Changes in the fractional coverages (see text for details) of phosphorus ($P/P_{D=0}$), fluorine ($F/F_{D=0}$), and platinum ($Pt/Pt_{D=0}$) atoms for adsorbed $Pt(PF_3)_4$ molecules as functions of electron dose (D). These spectra were acquired at 89 eV pass energy to maximize XPS intensity. Plots on the left-hand side are shown for all three elements over the full range of electron doses studied ($<2 \times 10^{17}$ e^-/cm^2); plots on the right-hand side are shown for just phosphorus and fluorine for the initial period of irradiation ($<3.0 \times 10^{15}$ e^-/cm^2). Solid lines through the experimental data are based on fits to a first-order loss process with the functional form $P/P_{D=0}$ (or $F/F_{D=0}$) $= B \exp(-\sigma D) + C$, where B and C are constants such that $B + C = 1$ and D is the electron dose. For phosphorus, fits are shown for the full range of electron doses studied, whereas for fluorine, fits are shown only for the initial period of irradiation.

order of 0.2−0.3 nA. The typical acquisition time of a HREEL spectrum was 30 min; during spectral acquisition, the accumulated electron dose from the HREELS incident beam was approximately 2 orders of magnitude smaller than the electron dose delivered by the flood gun.

B. Films Deposited at Room Temperature in a Partial Pressure of $Pt(PF_3)_4$. A film created by electron-beam-induced deposition of gas-phase $Pt(PF_3)_4$ was generated using the electron gun in an Auger electron spectrometer (Physical Electronics 610; LaB_6 filament; $P_{base} < 2 \times 10^{-9}$ Torr).[40,60] For this experiment, a sputter-cleaned polycrystalline Au foil was used as the substrate. The rectangularly shaped film was created by rastering the Auger electron beam (1.5 keV; ∼1.5-μm spot size) over the gold surface in a repetitive serpentine mode for 50 min in the presence of a reasonably constant partial pressure [(6.0−7.5) $\times 10^{-7}$ Torr] of $Pt(PF_3)_4$. In these experiments, the substrate was at ambient temperature (∼298 K) throughout the deposition process. The current density in these studies was estimated to be at least 10^4 greater than that used in the UHV surface science studies. Once deposited, the film's size and chemical composition were determined by Auger electron spectrometry (AES).

III. RESULTS

The bottom spectrum in Figure 1 shows HREELS data obtained for 3 ML of $Pt(PF_3)_4$ adsorbed on a polycrystalline Pt foil at a substrate temperature of 20−30 K. The various fundamental and multiple scattering modes observed are consistent with previous IR measurements of $Pt(PF_3)_4$,[61] and the assignment of a Pt—P stretching mode at 26 meV is based on HREELS studies of PF_3 adsorbed onto various metal surfaces.[62] Upon annealing to 140 K, a measurable but proportionate decrease in intensity was observed for all of the vibrational modes, consistent with some $Pt(PF_3)_4$ desorption from a multilayer state. When the annealed $Pt(PF_3)_4$ adlayer was subsequently exposed to 500 eV electrons (uppermost two HREEL spectra in Figure 1), the vibrational modes decreased in intensity and broadened as the electron dose increased. The peak position of the most intense mode, the PF_3 symmetric stretch was observed to undergo a red shift, from 114 to 107 meV.

Figure 2 shows representative XPS data that describe the influence of electron irradiation on the chemical composition and bonding environments of submonolayer coverages of $Pt(PF_3)_4$ adsorbed onto a-C substrates. The four spectral regions monitored correspond to the most intense and diagnostic transitions associated with the three elements present in the precursor (platinum, phosphorus, and fluorine), as well as oxygen, which appeared within the adlayer as a result of electron irradiation. XPS experiments were performed over a number of days on films with slightly different initial $Pt(PF_3)_4$ coverages (0.16 ML ± 5%) in the submonolayer regime. To compensate for slight day-to-day variations in film thicknesses due to differences in $Pt(PF_3)_4$ exposures, the XPS signal intensities in

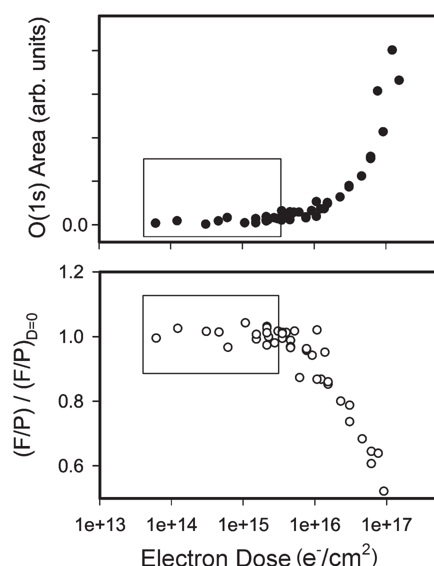

Figure 4. (Top) Uptake of oxygen and (bottom) change in the fluorine-to-phosphorus ratio (F/P) plotted as functions of electron dose (D). To accentuate the initial period of irradiation, the electron dose is plotted on a logarithmic scale. In each plot, the solid box represents the initial period of electron irradiation ($<3.0 \times 10^{15}$ e^-/cm^2).

Figure 2 were adjusted such that the Pt 4f peak area prior to irradiation remained constant from day to day. Consequently, Figure 2 reflects how electron irradiation changes both the intensity and the spectral envelopes in the four regions. Prior to irradiation, the Pt 4f region contains a well-separated doublet due to the Pt $4f_{7/2}$ and Pt $4f_{5/2}$ transitions within the parent $Pt(PF_3)_4$ molecule. The 74.4 eV peak position of the Pt $4f_{7/2}$ transition is indicative of Pt atoms in an oxidized state. The P 2p region consists of a single asymmetric feature due to a closely spaced $2p_{3/2}/2p_{1/2}$ doublet[63] with maximum peak intensity at 135.8 eV. Prior to electron irradiation, no spectral intensity was observed within the O 1s region, indicating that the substrate temperature was high enough to prevent adsorption of any residual water vapor remaining in the UHV chamber. In the F 1s region, a single symmetric peak was observed at 688.7 eV and ascribed to fluorine atoms in the PF_3 ligands. Thus, the XPS data are consistent with both the HREELS data and previous UHV studies,[64] indicating that, in the absence of electron beam irradiation, $Pt(PF_3)_4$ remains intact upon adsorption at these low substrate temperatures (<160 K). To provide additional insights into the structure of the adlayer prior to irradiation, XPS measurements were made to probe the variation in film thickness as a function of the $Pt(PF_3)_4$ dose (shown in Figure S1). These results indicate that the layer thickness appears to reach a limiting value of 0.3−0.4 nm at high doses, consistent with the existence of a discrete monolayer state at these temperatures (~160 K).[64] Based on the nonpolar nature of the a-C substrate and the lack of a molecular dipole in the $Pt(PF_3)_4$ adsorbate, it seems likely that the structure of the adlayer in the submonolayer regime consists of isolated $Pt(PF_3)_4$ molecules in coexistence with some two-dimensional islands.

Figure 2 also shows the changes within the Pt 4f, P 2p, F 1s, and O 1s regions as $Pt(PF_3)_4$ molecules are exposed to an increasing electron dose (D). The effects of electron irradiation on these various spectral regions can be conveniently divided up into electron doses less than or greater than $\sim 3 \times 10^{15}$ e^-/cm^2. For comparatively small electron doses ($\lesssim 3 \times 10^{15}$ e^-/cm^2), the most visible changes are the broadening of the Pt 4f spectral envelope to lower binding energy and the decrease in intensity within the P 2p and F 1s regions, although the shape of the spectral envelopes in these two regions remains largely unchanged. This regime is also characterized by a lack of intensity in the O 1s region. For electron doses $\gtrsim 3 \times 10^{15}$ e^-/cm^2, the Pt 4f envelope exhibits little change. In contrast, Figure 2 shows that the P 2p spectral envelope now begins to broaden significantly, reaching a maximum width at $\sim 3.7 \times 10^{16}$ e^-/cm^2 before sharpening again after even larger electron doses. As a result of electron irradiation, the P 2p peak position also shifts to lower binding energies, decreasing from its initial value of 135.8 to 133.6 eV after an electron dose of 3.3×10^{17} e^-/cm^2. In the range of electron doses $\gtrsim 3 \times 10^{15}$ e^-/cm^2, the F 1s peak position also continues to decrease in binding energy, although the most pronounced change is the decrease in intensity. In addition, a broad oxygen peak now appears with a peak between 532 and 533 eV. The intensity of this oxygen peak continues to increase as a function of electron dose, as shown in Figure 2.

In Figure 3, the fractional coverages of phosphorus ($P/P_{D=0}$), fluorine ($F/F_{D=0}$), and platinum ($Pt/Pt_{D=0}$) atoms are shown for adsorbed $Pt(PF_3)_4$ molecules plotted as functions of electron dose (D). The fractional coverage of each element was obtained by integrating the area of the spectral envelopes within the P 2p, F 1s, or Pt 4f region, recorded at 89 eV pass energy to optimize the signal-to-noise ratio at the expense of spectral resolution. These data were then compared to the value measured for the same spectral transition on the same film prior to electron irradiation ($D = 0$) to determine the fractional coverage. Analysis of Figure 3 reveals that electron exposure produces different changes in the fractional coverages of the three constituent elements of $Pt(PF_3)_4$: platinum, phosphorus, and fluorine. For electron doses $\lesssim 3 \times 10^{15}$ e^-/cm^2, $P/P_{D=0}$ and $F/F_{D=0}$ exhibit similar dependences on electron dose, decreasing to ~0.75 of their initial values (two uppermost plots on the right-hand side of Figure 3). Indeed, the loss of fluorine and phosphorus atoms in this regime can be well-described by a first-order kinetic process (fits shown as solid lines) with similar reaction cross sections ($\sigma_F = 2.1 \times 10^{15}$ cm^2 and $\sigma_P = 2.8 \times 10^{15}$ cm^2). However, for electron doses $\gtrsim 3 \times 10^{15}$ e^-/cm^2, changes in the fractional coverages of fluorine and phosphorus atoms are no longer correlated. Thus, although ($P/P_{D=0}$) remains unchanged for electron doses $\gtrsim 3 \times 10^{15}$ e^-/cm^2, ($F/F_{D=0}$) continues to decrease. In contrast to the behavior of $P/P_{D=0}$ or $F/F_{D=0}$, $Pt/Pt_{D=0}$ remains essentially constant over the full range of electron doses.

Figure 4 shows how the O 1s XPS area (top) and the fluorine-to-phosphorus ratio (F/P) (bottom) change as functions of electron dose. To allow changes in these variables to be discerned for both comparatively small and larger electron doses, the x axis in Figure 4 is shown on a logarithmic scale. In each plot, the box represents the initial period of irradiation where the electron dose is $\lesssim 3 \times 10^{15}$ e^-/cm^2. Analysis of Figure 4 reveals that the O 1s XPS signal remains very close to zero within the boxed region that corresponds to the initial stages of the electron-induced reactions but increases rapidly for electron doses $\gtrsim 3 \times 10^{15}$ e^-/cm^2, consistent with the qualitative changes observed within the O 1s region shown in Figure 2. The F/P ratio within the adlayer also exhibits a systematic and well-defined dependence on electron dose; for electron doses $\lesssim 3 \times 10^{15}$ e^-/cm^2, the F/P ratio remains unchanged compared to the value in the parent $Pt(PF_3)_4$ molecules, but it then decreases systematically for larger electron doses.

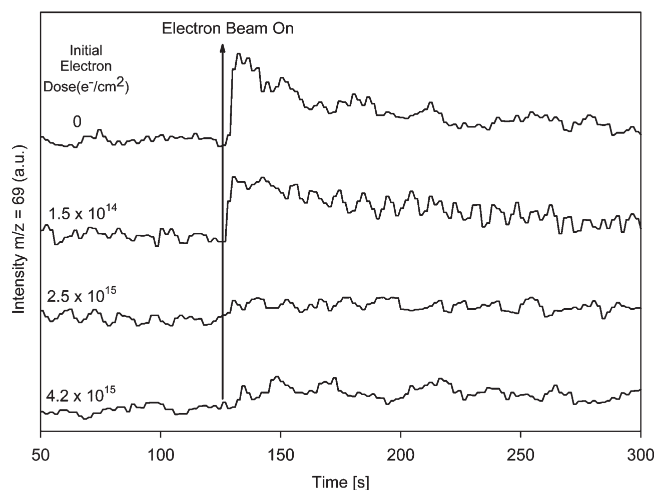

Figure 5. Time-based mass spectra showing the evolution of gas-phase PF_3 (as measured by the PF_2^+ fragment at $m/z = 69$) for $Pt(PF_3)_4$ films exposed to 500 eV electrons. (See text for details of film preparation and irradiation conditions.) In each trace, the solid vertical line indicates the time at which the electron beam was turned on, and the initial electron dose represents the electron dose that the film had been exposed to before the time-based trace was acquired.

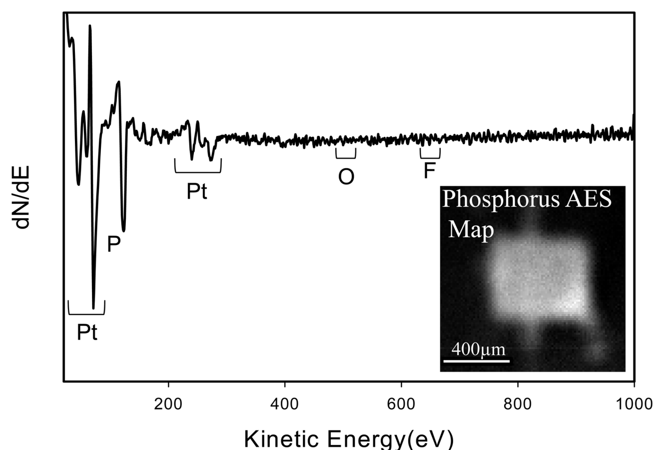

Figure 6. Auger spectrum of a film deposited by electron irradiating a sputter-cleaned gold substrate in the presence of $Pt(PF_3)_4$. Deposition conditions were: total deposition time = 60 min, $P_{Pt(PF_3)_4} \approx 6.5 \times 10^{-7}$ Torr, incident beam energy = 1.5 keV, substrate current = 0.1 mA. Inset shows a phosphorus map of the EBID structure.

Neutral fragments ejected into the gas phase during electron irradiation of adsorbed $Pt(PF_3)_4$ at ~160 K were probed by quadrupole mass spectrometry (QMS). Figure 5 shows the results obtained by monitoring $m/z = 69$, the m/z value that corresponds to PF_2, the largest peak produced by electron impact ionization of either PF_3 or $Pt(PF_3)_4$.[65] Results that are similar to (but noisier than) those shown in Figure 5 were obtained by monitoring $m/z = 88$, corresponding to PF_3 (data not shown). In these experiments, slightly thicker $Pt(PF_3)_4$ films were deposited (film thicknesses of 0.35 nm/0.47 ML, created by using 15 L exposures), and higher target currents (45 μA) were used to boost the $m/z = 69$ signal generated by electron irradiation to a level distinguishable from the background noise (see Figure 5). Furthermore, to ensure that the QMS data could be directly compared between different experiments, the initial $Pt(PF_3)_4$ dose was carefully controlled to ensure that the initial film thicknesses were similar (±10%). The protocol for these experiments was as follows: After $Pt(PF_3)_4$ deposition, the adlayer was exposed to a well-defined initial electron dose (indicated on the left-hand side of each spectrum in Figure 5). Following this period of preirradiation, the adlayer was once again exposed to electron irradiation, whose onset is shown by the vertical arrow in Figure 5, and the $m/z = 69$ signal was subsequently monitored. Figure 5 shows that there was a measurable increase in the $m/z = 69$ signal upon electron irradiation of $Pt(PF_3)_4$ films that received no pre-irradiation, although the signal intensity decayed as a function of increasing irradiation time. A smaller, but still measurable increase in the $m/z = 69$ signal was observed when $Pt(PF_3)_4$ adlayers pre-exposed to an electron dose of 1.5×10^{14} e^-/cm^2 were subsequently irradiated. However, for $Pt(PF_3)_4$ adlayers pre-exposed to an electron dose of either 2.5×10^{15} or 4.2×10^{15} e^-/cm^2, there was no discernible increase in the $m/z = 69$ signal upon subsequent irradiation (bottom spectra in Figure 5).

Figure 6 shows the in situ AE spectrum of an ~500 μm × 700 μm film deposited in the AES system in the presence of a constant partial pressure of $Pt(PF_3)_4$ onto a Au substrate at ~298 K. Principal AES peaks associated with deposited platinum and phosphorus atoms are clearly observed at 64 and 120 eV, respectively. However, there is no evidence of any diagnostic AES peaks due to either fluorine or oxygen atoms, which would appear at 647 and 510 eV, respectively. The inset in Figure 6 is an AES map of the phosphorus signal, which shows that the deposit is localized within the region of electron irradiation. The slight irregularities in the shape of the deposit can be ascribed to deviations in the raster pattern.

IV. DISCUSSION

In conjunction, the XPS, MS, and HREELS data presented in the Results section enable the construction of a detailed picture of the elementary bond-breaking steps and reactions involved in the electron-induced decomposition of $Pt(PF_3)_4$. In summary, the reaction proceeds in two discrete stages: The initial step involves electron-stimulated cleavage of one of the four PF_3 ligands and ejection of the free PF_3 ligand into the gas phase. However, further decomposition of the platinum precursor proceeds through P—F rather than Pt—P bond cleavage, leading to the release of fluorine into the gas phase and the concomitant reaction of undercoordinated phosphorus atoms with water vapor to generate phosphorus—oxygen bonds in the film.

Step 1: Pt—P Bond Cleavage and PF_3 Release. In this regime, characterized by electron doses $\lesssim 3 \times 10^{15}$ e^-/cm^2, the overall chemical reaction can be represented as

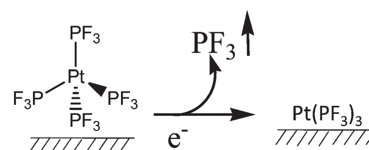

Experimental evidence for the electron-stimulated ejection of one PF_3 ligand from each precursor molecule can be found in the XPS data shown in Figure 3. Specifically, the fractional coverages of phosphorus and fluorine atoms decrease to almost exactly three-quarters of their initial values during these early stages of

the reaction, whereas the fractional coverage of platinum atoms and the F/P ratio (Figure 4) remain constant, the latter providing clear evidence that the losses of these two elements from the adlayer are correlated. It should also be noted that the lack of change in platinum atom coverage over the entire range of electron doses (Figure 3) indicates that electron irradiation produces only chemical transformations in the absence of any molecular $Pt(PF_3)_4$ desorption, consistent with previous EBID studies.[39,40] Furthermore, by measuring the Pt 4f region before and after electron irradiation, we also verified that this lack of electron-stimulated $Pt(PF_3)_4$ desorption persisted for MS experiments (Figure 5), which were performed using higher target currents.

Other experimental data are also consistent with the hypothesis that the initial bond-breaking event involves Pt—PF_3 bond cleavage. For example, the shapes of the P 2p and F 1s spectral envelopes remain virtually unchanged for electron doses $\lesssim 3 \times 10^{15}$ e^-/cm^2 (bottom three spectra in Figure 2), despite the obvious loss of spectral intensity. The electron-stimulated loss of PF_3 ligands is also consistent with the decrease in the intensities of the P—F and Pt—P vibrational modes observed by HREELS in Figure 1; the increase in peak widths can be ascribed to an increase in heterogeneity within the film caused by the creation of an adlayer that consists of a mixture of species. Finally, QMS data indicate that, when $Pt(PF_3)_4$ films are initially exposed to electron irradiation, a species that produces fragments at m/z = 69 (Figure 5) and m/z = 88 is ejected into the gas phase, the latter corresponding to the molecular weight of PF_3. In principle, this species could arise from the ejection of either PF_3 or $Pt(PF_3)_4$, but the lack of electron-stimulated $Pt(PF_3)_4$ desorption (see Figures 2 and 3), indicates that it is PF_3 being released into the gas phase. Thus, Figure 5 shows that PF_3 ejection is restricted to electron doses of $\lesssim 3 \times 10^{15}$ e^-/cm^2, consistent with the regime where losses of phosphorus and fluorine atoms from the adlayer are correlated (Figures 3 and 5).

It is also worth noting that this initial Pt—PF_3 bond-breaking step in the electron-stimulated decomposition of adsorbed $Pt(PF_3)_4$ is analogous to the effect of thermal electrons on $Pt(PF_3)_4$ and $Ni(PF_3)_4$ in the gas phase.[66] Using negative-ion MS, this study showed that one PF_3 ligand was lost from the tetrakis(trifluorophosphine) transition-metal complexes by identifying the production of $M(PF_3)_3^-$. For $Ni(PF_3)_4$, the authors used density functional theory (DFT) to show that the production of $Ni(PF_3)_3^-$ by dissociative electron attachment was exothermic by >0.8 eV. Thus, we postulate that the surface-bound tetrakis(trifluorophosphine)platinum transition-metal complex undergoes a similar initial decomposition step, with the only difference being the almost certain and rapid charge neutralization of the surface-bound $Pt(PF_3)_3^-$ anion on a conducting substrate. It also seems likely that a single Pt—PF_3 bond-cleavage event represents the first elementary reaction step involved in UV-laser metallization studies using $Pt(PF_3)_4$, because low-energy electrons are presumed to play an essential role in initiating deposition in this process.[34]

The deposition and growth of nanostructures in typical focused electron-beam-induced processing occurs in the presence of a constant partial pressure of precursor molecules, with a substrate temperature of ~298 K.[1−4] Under these conditions, it is very difficult to quantify reaction cross sections. However, based on the results from our UHV surface science approach, we were able to determine that, in electron-beam-induced processing, *deposition* of $Pt(PF_3)_4$ is controlled by the initial Pt—PF_3 bond-cleavage step, which effectively converts gas-phase $Pt(PF_3)_4$ into a surface-bound species. Because the initial coverage of $Pt(PF_3)_4$ molecules is fixed in our experiments, we would anticipate that, in this initial step, the loss of PF_3 ligands (as reflected by the decrease in $P/P_{D=0}$ and $F/F_{D=0}$) should follow first-order kinetics with respect to electron dose. Consistent with this hypothesis, the decreases in $P/P_{D=0}$ and $F/F_{D=0}$ observed in XPS for electron doses $\lesssim 3 \times 10^{15}$ e^-/cm^2 can be well fit by pseudo-first-order loss processes (shown as the solid lines in the plots on the right-hand side of Figure 3). In FEBIP, when deposition occurs in the precursor-limited regime, growth rates are typically proportional to the electron fluence, indicating that the rate of electron-stimulated deposition involves a one-electron process. Consequently, the rate of $Pt(PF_4)_3$ loss in our UHV surface science studies, expressed as a function of the electron dose, corresponds to the reaction cross section, which, for $Pt(PF_3)_4$ deposition onto a-C substrates using an incident electron energy of 500 eV, is ~2.5×10^{-15} cm^2. This value was determined by averaging the cross-section values obtained by measuring the losses of phosphorus and fluorine atoms for electron doses of $\lesssim 3 \times 10^{15}$ e^-/cm^2.

Step 2: P—F Bond Cleavage and Phosphorus Oxidation. For electron doses $\gtrsim 3 \times 10^{15}$ e^-/cm^2, we postulate that the remaining $Pt(PF_3)_3$ species lose fluorine as a consequence of P—F bond cleavage, whereas the coordinatively unsaturated phosphorus atoms left behind are rapidly oxidized by water. The overall processes can be represented as

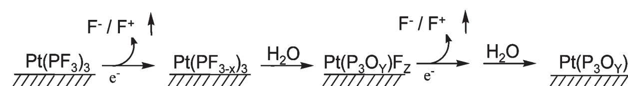

The clearest evidence for the onset of P—F bond cleavage again comes from the XPS data shown in Figures 2−4. Analysis of these figures reveals that, for electron doses $\gtrsim 3 \times 10^{15}$ e^-/cm^2, although the fractional coverage of phosphorus atoms remains unchanged at ~0.75 of its nascent value, the fluorine coverage (Figure 3) and F/P ratio (Figure 4) both begin to decrease systematically with increasing electron dose. Collectively, these results point toward a loss of fluorine atoms from the remaining PF_3 ligands. Indeed, previous electron-stimulated desorption (ESD) studies have shown that electron irradiation of PF_3 adsorbed onto various metal surfaces yields both F^+ and F^- species.[67−72] As a consequence of this electron-activated fluorine stripping, coordinatively unsaturated phosphorus atoms are created within the adlayer that then react with residual water vapor in the UHV chamber, driven by the thermodynamic strength of phosphorus oxygen bonds (P═O and P—O bond strengths are ~550 and 350 kJ mol^{-1}, respectively[73]). This assertion is supported by the observation that oxygen uptake into the film (shown in Figures 2 and 4) is observed only for electron doses $\gtrsim 3 \times 10^{15}$ e^-/cm^2, correlated with the onset of the coordinatively unsaturated phosphorus atoms being created. Consistent with this hypothesis, for electron doses $\gtrsim 3 \times 10^{15}$ e^-/cm^2, where reactions are a consequence of the interactions of electrons with adsorbed $Pt(PF_3)_3$ species, the increase in oxygen signal intensity and the corresponding decrease in fluorine intensity exhibit similar functional dependences on the electron dose. Further support for this idea is provided by results from studies performed as part of this investigation in which a $Pt(PF_3)_4$ film that had been exposed to an electron dose of ~3×10^{15} e^-/cm^2 was left in the UHV chamber for several hours as

the substrate temperature was held constant. XPS analysis revealed that no measurable oxygen uptake occurred in this experiment, indicating that the $Pt(PF_3)_3$ species formed after an electron dose of $\sim 3 \times 10^{15}$ e^-/cm^2 remains stable at ~160 K and that the uptake of oxygen into the film is correlated solely with the electron dose and the creation/reactivity of the coordinatively unsaturated phosphorus atoms. Although we have not attempted to quantify the reaction cross section for fluorine loss from the adsorbed $Pt(PF_3)_3$ species, analysis of the data in Figure 3 indicates that the rate of electron-stimulated P—F bond cleavage is significantly lower than that of the initial Pt—P bond cleavage event.

Changes in the shape of the P 2p transition for electron doses $\gtrsim 3 \times 10^{15}$ e^-/cm^2, in particular, also reflect the chemical transformations described in the previous paragraph. Thus, although the P 2p spectral envelopes remained qualitatively unchanged in terms of shape for electron doses $\lesssim 3 \times 10^{15}$ e^-/cm^2 for which reactions lead to PF_3 ligand desorption, for larger electron doses, Figure 2 shows that the P 2p spectrum broadens and shifts to lower binding energies. This can be rationalized by the effective transition from P—F to P—O/P═O bonding in the inorganic film as the highly electronegative fluorine atoms are removed through electron-stimulated P—F bond cleavage and the coordinately unsaturated phosphorus atoms that are created react with residual water vapor. In support of this assertion, both the P 2p and O 1s regions after prolonged irradiation are qualitatively similar in terms of both shape and peak positions to those of the oxidized phosphorus species observed in previous studies when carbon phosphide films were oxidized.[74] Analysis of the P 2p region for electron doses $\gtrsim 3 \times 10^{15}$ e^-/cm^2 also reveals that the width of the spectral envelope broadens considerably before sharpening again at the highest electron doses studied. (See, for example, a comparison of the P 2p spectra recorded for electron doses of 3.7×10^{16} and 3.3×10^{17} e^-/cm^2 in Figure 2.) Again, this phenomenon can be rationalized by the changes to the local bonding environment that the phosphorus atoms experience as a consequence of irradiation. At the onset of P—F bond cleavage and the concomitant phosphorus oxidation, an extremely heterogeneous distribution of phosphorus atoms is created in the film, ranging from residual PF_3 groups to partially oxidized species such as PF_2O and PFO. Each of these types of species gives rise to a slightly different binding energy for the associated phosphorus atom, leading to a broad P 2p spectral envelope. Upon further irradiation, ever-increasing fractions of the fluorine atoms have been removed, increasing the homogeneity of local chemical environments in the film and decreasing the width of the P 2p spectral envelope.

The other analytical techniques employed in this study (MS and HREELS) also support the idea that P—F bond cleavage predominates during the second phase of the decomposition process. For example, Figure 5 shows that no gas-phase PF_3 was observed for $Pt(PF_3)_4$ films that had been exposed to an initial electron dose of 4.2×10^{15} e^-/cm^2, a value sufficient to convert all adsorbed $Pt(PF_3)_4$ molecules to $Pt(PF_3)_3$. Electron-stimulated reactions of these $Pt(PF_3)_3$ species are postulated to lead exclusively to P—F bond cleavage and the loss of F^- and F^+ species. In terms of the HREELS data, Figure 1 shows that electron irradiation leads to a decrease in spectral intensity for vibrational modes associated with the P—F groups, as well as a red shift in the peak position of the P—F stretching mode. Both of these observations are consistent with the loss of PF_3 and production of PF_x species ($x < 3$). For example, based on matrix isolation studies,[75] the peak position of the P—F symmetric stretching mode in PF_2 as compared to PF_3 red shifts by ~5 meV,[76,67] similar to the ~8 meV decrease in peak position observed in Figure 1 when $Pt(PF_3)_4$ molecules were exposed to electron irradiation.

In EBID studies, a particularly important facet is the change to the local chemical environment/oxidation state of the metal center. During the first stage of the reaction, in which a single electronegative PF_3 ligand is ejected, the Pt 4f peak position decreases by ~1.0 eV to a lower binding energy. In contrast, there is little or no change to the binding energy of the Pt 4f peaks during stage 2 of the electron-stimulated decomposition, even though the electron dose increases by 2 orders of magnitude from $\sim 3 \times 10^{15}$ to 3×10^{17} e^-/cm^2. This can be ascribed to the fact that, even though the local bonding on the remaining phosphorus atoms is being transformed from P—F to P—O, the central platinum atoms are still involved in Pt—P bonding. This is also consistent with the fact that the Pt 4f peak position for metallic Pt has previously been measured to be 71.1 eV in the same apparatus, almost 1.5 eV lower than the lowest Pt $4f_{7/2}$ binding energy observed in the present study.[39]

Insights obtained from our low-temperature UHV surface science studies can be used to help rationalize some aspects of film composition that characterize EBID structures created using $Pt(PF_3)_4$ in electron microscopes and AES systems (e.g., Figure 6). In these typical EBID experiments, structures are grown at substrate temperatures of ~298 K using a focused electron beam in the presence of a constant partial pressure of precursor molecules.[1−4] Under these conditions, the coverage of precursor molecules is determined by a dynamic equilibrium governed by the rates of adsorption from the gas phase and thermal desorption of adsorbed precursor molecules. In terms of the electron-stimulated deposition step, our UHV surface science studies have shown that this occurs as a result of Pt—P bond cleavage, the loss of one PF_3 ligand, and the creation of a surface-bound $Pt(PF_3)_3$-type species. The identification of this elementary process not only allows for the determination of the deposition cross section ($\sigma_{Pt(PF_3)_4}$) but also helps to rationalize why the Pt/P ratio in EBID films created from $Pt(PF_3)_4$ is always greater than that of the precursor, regardless of the deposition conditions.[28,29,31] Thus, the platinum-containing films deposited at room temperature in the presence of a constant partial pressure of $Pt(PF_3)_4$ exhibited a Pt/P ratio of ~2/1 as determined from the peak-to-peak ratios of the platinum and phosphorus peaks (corrected for relative sensitivity factors) in Figure 6. Furthermore, the second stage of the electron-induced decomposition process predicts that sufficiently large electron doses should remove all of the fluorine atoms from the film, through P—F bond cleavage and fluorine release. Consistent with this hypothesis, the platinum-containing film shown in Figure 6, which certainly experienced an orders-of-magnitude higher electron dose than films created in the UHV surface science studies, does not contain any fluorine. Similar results have also been reported for EBID films created from $Pt(PF_3)_4$ in other AES systems or in electron microscopes.[28,29] Interestingly, the platinum-containing film in Figure 6 does not show any evidence of oxygen uptake, in contrast to the results obtained in the XPS system. This is almost certainly a consequence of the very low background pressure of water in the AES system ($P_{base} < 2 \times 10^{-9}$ Torr) and the fact that deposition was performed at room temperature rather than ~160 K as in the XPS

experiments. Both of these sets of deposition conditions will reduce the occurrence of phosphorus oxidation. However, significant amounts of oxygen are almost always observed in EBID nanostructures created from $Pt(PF_3)_4$ using electron microscopes, where, although the substrate is at ~298 K, the base pressure during deposition is typically only $10^{-5}-10^{-6}$ Torr. This suggests that the partial pressure of water vapor affects the oxygen content in the deposited film, an assertion supported by observations of Botman, who noticed a qualitative correlation between the oxygen content in EBID films deposited from $Pt(PF_3)_4$ in a high-vacuum electron microscope and the partial pressure of water in the chamber.[31] Based on data obtained in the present investigation, the creation of coordinatively unsaturated phosphorus atoms by P—F bond cleavage and their subsequent reactions with residual water vapor provides a mechanistic rationale for the oxygen uptake.

In terms of the bond-breaking steps involved in electron-stimulated deposition, some interesting similarities become apparent when the results of the present UHV data are compared to those recently acquired on another monodentate EBID precursor, trimethyl(methylcyclopentadienyl) platinum ($MeCpPtMe_3$).[39] For both $Pt(PF_3)_4$ and $MeCpPtMe_3$, the initial electron-stimulated reaction involves cleavage of a single metal–ligand bond and ejection of the "free" ligand into the gas phase.[39,41] In the case of $MeCpPtMe_3$, this involves electron-stimulated Pt—CH_3 bond breaking. For both precursors, these initial bond-breaking steps (Pt—PF_3 and Pt—CH_3) are analogous to the purely thermal processes involved in chemical vapor deposition (CVD) of the same precursors.[77] Thus, the ability to deposit almost pure platinum films in CVD processes using $Pt(PF_3)_4$ indicates that thermal decomposition follows exclusive Pt—PF_3 bond cleavage.[32] However, during electron-induced reactions, ligands that remain after the initial, single-ligand ejection step are not released intact into the gas phase as they are in CVD but, in contrast, undergo electron-stimulated decomposition. Consequently, electron-induced decomposition of $Pt(PF_3)_4$ and $MeCpPtMe_3$ ultimately leaves 75 and 89 at. % of the nascent phosphorus and carbon atoms, respectively, associated with the precursor becoming incorporated into the deposit.[39] We are currently investigating the extent to which this pattern of electron-stimulated reactivity can be generalized to other types of monodentate organometallics (e.g., metal carbonyls) that are also widely used as EBID precursors.[78−81]

Perhaps the most interesting observation of the present study is the shift from Pt—P to P—F bond cleavage that occurs following the loss of a single PF_3 ligand from each adsorbed $Pt(PF_3)_4$ molecule. The reason for this abrupt shift in decomposition mechanism following the initial electron-stimulated ligand ejection step has not been unambiguously determined. One possibility is that this shift in reaction mechanism is a consequence of the conversion of gas-phase $Pt(PF_3)_4$ species into a surface-bound $Pt(PF_3)_3$ moiety, whose electron-stimulated reactions are altered by its adsorbed state compared to those of the parent molecule. This discussion underscores the need for a more detailed theoretical understanding of the bond-breaking events that accompany the electron-stimulated decomposition of adsorbed precursors, including the nature of the excitation process. However, except for a few isolated cases, experimental information on electron-stimulated reactions with even gas-phase organometallic species used in EBID is extremely sparse.[66] Another unresolved question is the exact nature of the electrons that are responsible for decomposition. In principle, the electron-stimulated decomposition of an adsorbed EBID precursor could be initiated either by the primary electron or by the low-energy secondary/backscattered electrons generated by the interaction of the primary electron beam with the substrate.

V. CONCLUSIONS

The electron-induced decomposition of adsorbed tetrakis(trifluorophosphine)platinum [$Pt(PF_3)_4$] molecules proceeds in two discrete stages. The initial deposition step, which occurs with a reaction cross section of $\sim 2.5 \times 10^{-15}$ cm^2 for 500 eV incident electrons, involves the selective cleavage of one Pt—PF_3 bond and the ejection of the intact PF_3 ligand into the gas phase. Subsequent electron-stimulated reactions of the $Pt(PF_3)_3$-type species that forms as a result of this initial step are, however, characterized by P—F rather than further Pt—P bond cleavage. In this second stage of the reaction, coordinately unsaturated phosphorus atoms created by P—F cleavage are oxidized by reactions with residual water vapor in the chamber. Taken in conjunction with recent data obtained on other monodentate EBID precursors (e.g., $MeCpPtMe_3$), results from the present study suggest that a common pattern of electron-stimulated reactivity exists for monodentate organometallic precursors, specifically, an initial step that involves ejection of a single ligand, followed by electron-stimulated decomposition of the residual ligands and their incorporation into the deposit. Insights obtained from our low-temperature UHV surface science studies also helped to rationalize some aspects of film composition observed for nanostructures created from $Pt(PF_3)_4$ in electron microscopes.

■ ASSOCIATED CONTENT

Supporting Information. Variation in the thickness of the $Pt(PF_3)_4$ film deposited as a function of the $Pt(PF_3)_4$ exposure as measured by XPS (Figure S1). Effect of X-ray irradiation alone on a $Pt(PF_3)_4$ film as measured by changes in the Pt 4f, P 2p, O 1s, and F 1s XPS transitions (Figure S2). Data for both Figures S1 and S2 were recorded in the apparatus used at Johns Hopkins University. This information is available free of charge via the Internet at http://pubs.acs.org.

■ AUTHOR INFORMATION

Corresponding Author
*E-mail: howardf@jhu.edu.

■ ACKNOWLEDGMENT

The authors acknowledge support provided by the DFG through Grant Sw26/13-1 and the COST Action CM0601 "Electron Controlled Chemical Lithography" (ECCL). The researchers from JHU and TU Delft also acknowledge Hans Mulders of FEI for transferring our precursor in his glovebox and for helpful tips on handling the $Pt(PF_3)_4$ precursor. The authors would also like to acknowledge the Material Science Department at JHU for use of the Auger electron spectrometer.

■ REFERENCES

(1) Randolph, S. J.; Fowlkes, J. D.; Rack, P. D. *Crit. Rev. Solid State Mater. Sci.* **2006**, *31*, 55.
(2) van Dorp, W. F.; Hagen, C. W. *J. Appl. Phys.* **2008**, *104*, 081301/1.

(3) Utke, I.; Hoffman, P.; Melngailis, J. *J. Vac. Sci. Technol. B* **2008**, *26*, 1197.
(4) Utke, I.; Gölzhäuser, A. *Angew. Chem., Int. Ed.* **2010**, *49*, 9328.
(5) Frey, L.; Lehrer, C.; Ryssel, H. *Appl. Phys. A: Mater. Sci. Process* **2003**, *76*, 1017.
(6) Igaki, J. Y.; Kanda, K.; Haruyama, Y.; Ishida, M.; Ochiai, Y.; Fujita, J. I.; Kaito, T.; Matsui, S. *Microelectron. Eng.* **2006**, *83*, 1225.
(7) Fujii, T.; Iwasaki, K.; Muekane, M.; Takeuchi, T.; Hasuda, M.; Asahata, Y.; Kyohara, M.; Kogure, T.; Kijima, Y.; Kaito, T. *J. Micromech. Microeng.* **2005**, *15*, S286.
(8) Lepore, A. Electron-Beam ULSI Applications. In *Handbook of VLSI Microlithography: Principles, Technology and Applications*, 2nd ed.; Helbert, J. N., Ed.; Noyes Publications/William Andrew Publishing: New York, 2001; Chapter 7, pp 670−755.
(9) Bakshi, V. *EUV Lithography*; SPIE/Wiley Interscience: New York, 2009.
(10) Mackus, A. J. M.; Mulders, J. J. L.; van de Sanden, M. C. M.; Kessels, W. M. M. *J. Appl. Phys.* **2010**, *107*, 116102/1.
(11) Perentes, A.; Hoffmann, P. *Chem. Vap. Depos.* **2007**, *13*, 176.
(12) Edinger, K.; Becht, H.; Bihr, J.; Boegli, V.; Budach, M.; Hofmann, T.; Koops, H. W. P.; Kuschnerus, P.; Oster, J.; Spies, P.; Weyrauch, B. *J. Vac. Sci. Technol. B* **2004**, *22*, 2902.
(13) Liang, T.; Frendberg, E.; Lieberman, B.; Stivers, A. *J. Vac. Sci. Technol. B* **2005**, *23*, 3101.
(14) Liang, T.; Stivers, A. *Proc. SPIE* **2002**, *4688*, 375.
(15) Utke, I.; Jenke, M. G.; Röling, C.; Thiesen, P. H.; Iakovlev, V.; Sirbu, A.; Mereuta, A.; Caliman, A.; Kapon, E. *Nanoscale* **2011**, *3*, 2718.
(16) Hubner, B.; Koops, H. W. P.; Pagnia, H.; Sotnik, N.; Urban, J.; Weber, M. *Ultramicroscopy* **1992**, *42−44*, 1519.
(17) Chen, I.-C.; Chen, L.-H.; Orme, C.; Quist, A.; Lal, R.; Jin, S. *Nanotechnology* **2006**, *17*, 4322.
(18) Frabboni, S.; Gazzadi, G. C.; Spessot, A. *Physica E* **2007**, *37*, 265.
(19) Hagen, C. W.; van Dorp, W. F.; Crozier, P. A. *J. Phys.: Conf. Ser.* **2008**, *126*, 012025/1.
(20) Rack, P. D.; Fowlkes, J. D.; Randolph, S. J. *Nanotechnology* **2007**, *18*, 465602.
(21) Kulshrestha, N.; Misra, A.; Srinivasan, S.; Hazra, K. S.; Bajpai, R.; Roy, S.; Vaidya, G.; Misra, D. S. *Appl. Phys. Lett.* **2010**, *97*, 222102/1.
(22) Li, P. G.; Jin, A. Z.; Tang, W. H. *Phys. Status Solidi A* **2006**, *203*, 282.
(23) Shimojo, M.; Takeguchi, M.; Mitsuishi, K.; Tanaka, M.; Furuya, K. *J. Phys.: Conf. Ser.* **2008**, *100*, 052016.
(24) Botman, A.; Mulders, J. J. L.; Hagen, C. W. *Nanotechnology* **2009**, *20*, 372001.
(25) Botman, A.; Hesselberth, M.; Mulders, J. J. L. *Microelectron. Eng.* **2008**, *85*, 1139.
(26) Botman, A.; Mulders, J. J. L.; Weemaes, R.; Mentink, S. *Nanotechnology* **2006**, *17*, 3779.
(27) Koops, H. W.; Kaya, A.; Weber, M. *J. Vac. Sci. Technol. B* **1995**, *13*, 2400.
(28) Barry, J. D.; Ervin, M. H.; Molstad, J.; Wickenden, A.; Brintinger, T.; Hoffman, P.; Meingailis, J. *J. Vac. Sci. Technol. B* **2006**, *24*, 3165.
(29) Wang, S.; Sun, Y. M.; Wang, Q.; White, J. M. *J. Vac. Sci. Technol. B* **2004**, *22*, 1803.
(30) Botman, A.; Hesselberth, M.; Mulders, J. J. L. *J. Vac. Sci. Technol. B* **2008**, *26*, 2464.
(31) Botman, A. P. J. M. Towards High Purity Nanostructures from Electron Beam Induced Deposition of Platinum. Ph.D. Thesis, Delft University of Technology, Delft, The Netherlands, 2009.
(32) Rand, M. J. *J. Electrochem. Soc.* **1973**, *120*, 686.
(33) Hsu, D. S. Y.; Troilo, L. M.; Turner, N. H.; Pierson, K. W. *Thin Solid Films* **1995**, *269*, 21.
(34) Schroder, H.; Kompa, K. L.; Masci, D.; Gianinoni, I. *Appl. Phys. A* **1985**, *38*, 227.
(35) Botman, A.; Hagen, C. W.; Li, J.; Thiel, B. L.; Dunn, K. A.; Mulders, J. J. L.; Randolph, S.; Toth, M. *J. Vac. Sci. Technol. B* **2009**, *27*, 2759.
(36) Ervin, M. H.; Chang, D.; Nichols, B.; Wickenden, A.; Barry, J.; Melngailis, J. *J. Vac. Sci. Technol. B* **2007**, *25*, 2250.
(37) Takeguchi, M.; Shimojo, M.; Furuya, K. *Appl. Phys. A* **2008**, *93*, 439.
(38) van Dorp, W. F.; Wnuk, J. D.; Gorham, J. M.; Fairbrother, D. H.; Madey, T. E.; Hagen, C. W. *J. Appl. Phys.* **2009**, *106*, 074903/1.
(39) Wnuk, J. D.; Gorham, J. M.; Rosenberg, S. G.; van Dorp, W. F.; Madey, T. E.; Hagen, C. W.; Fairbrother, D. H. *J. Phys. Chem. C* **2009**, *113*, 2487.
(40) Wnuk, J. D.; Gorham, J. M.; Rosenberg, S. G.; van Dorp, W. F.; Madey, T. E.; Hagen, C. W.; Fairbrother, D. H. *J. Appl. Phys.* **2010**, *107*, 054301/1.
(41) Wnuk, J. D.; Rosenberg, S. G.; Gorham, J. M.; van Dorp, W. F.; Hagen, C. W.; Fairbrother, D. H. *Surf. Sci.* **2011**, *605*, 257.
(42) Randolph, S. J.; Fowlkes, J. D.; Rack, P. D. *J. Appl. Phys.* **2005**, *97*, 124312.
(43) Mezhenny, S.; Lyubinetsky, I.; Choyke, W. J.; Yates, J. T. *J. Appl. Phys.* **1999**, *85*, 3368.
(44) Henderson, M. A.; Ramsier, R. D.; Yates, J. T. *Surf. Sci.* **1991**, *259*, 173.
(45) Henderson, M. A.; Ramsier, R. D.; Yates, J. T. *J. Vac. Sci. Technol. A* **1991**, *9*, 1563.
(46) Ramsier, R. D.; Henderson, M. A.; Yates, J.T., Jr. *Surf. Sci.* **1991**, *257*, 9.
(47) Ramsier, R. D.; Yates, J.T., Jr. *Surf. Sci.* **1993**, *289*, 39.
(48) Swiderek, P.; Jäggle, C.; Bankmann, D.; Burean, E. *J. Phys. Chem. C* **2007**, *111*, 303.
(49) Swiderek, P. *Eur. Phys. J. D* **2005**, *35*, 355.
(50) Breton, S.-P.; Michaud, M.; Jäggle, C.; Swiderek, P.; Sanche, L. *J. Chem. Phys.* **2004**, *121*, 11240.
(51) Weeks, L. D.; Zhu, L. L.; Pellon, M.; Haines, D. R.; Arumainayagam, C. R. *J. Phys. Chem. C* **2007**, *111*, 4815.
(52) Harris, T. D.; Lee, D. H.; Blumberg, M. Q.; Arumainayagam, C. R. *J. Phys. Chem.* **1995**, *99*, 9530.
(53) Arumainayagam, C. R.; Lee, H.-L.; Nelson, R. B.; Haines, D. R.; Gunawardane, R. P. *Surf. Sci. Rep.* **2010**, *65*, 1.
(54) Hedhili, M. N.; Bredehoeft, J. H.; Swiderek, P. *J. Phys. Chem. C* **2009**, *113*, 13282.
(55) Tanuma, S.; Powell, C. J.; Penn, D. R. *Surf. Interface Anal.* **1991**, *17*, 911.
(56) Drews, T.; Rusch, D.; Seidel, S.; Willemsen, S.; Seppelt, K. *Chem.—Eur. J.* **2008**, *14*, 428.
(57) Swiderek, P.; Mann, A. *J. Electron Spectrosc. Relat. Phenom.* **2002**, *122*, 37.
(58) Moulder, J. F.; Stickle, W. F.; Sobol, P. E.; Bomben, K. D. *Handbook of X-ray Photoelectron Spectroscopy*; Physical Electronics USA, Inc.: Chanhassen, MN, 1995.
(59) Swiderek, P.; Winterling, H. *Chem. Phys.* **1998**, *229*, 295.
(60) Wnuk, J. D.; Gorham, J. M.; Rosenberg, S. G.; Madey, T. E.; Hagen, C. W.; Fairbrother, D. H. *J. Vac. Sci. Technol. B* **2010**, *28*, 527.
(61) Kruck, V. T.; Baur, K. *Z. Anorg. Allg. Chem.* **1969**, *364*, 192.
(62) Zhou, Y.; Mitchell, G. E.; Henderson, M. A.; White, J. M. *Surf. Sci.* **1989**, *214*, 209.
(63) Zhou, X. L.; White, J. M. *Surf. Sci.* **1989**, *221*, 534.
(64) Zhang, R.; Comita, P. B. *Chem. Phys. Lett.* **1992**, *200*, 297.
(65) Crozier, P. A.; Tolle, J.; Kouvetakis, J.; Ritter, C. *Appl. Phys. Lett.* **2004**, *84*, 3441.
(66) Friedman, J. F.; Miller, T. M.; Friedman-Schaffer, J. K.; Viggiano, A. A.; Rekha, G. K.; Stevens, A. E. *J. Chem. Phys.* **2008**, *128*, 104303.
(67) Madey, T. E.; Tao, H.-S.; Nair, L.; Diebold, U.; Shivapras, S. M.; Johnson, A. L.; Pradzisz, A.; Shinn, N. D.; Yarmoff, J. A.; Chakarian, V.; Shuh, D. Structure and kinetics of electron beam damage in a chemisorbed monolayer: PF_3 on Ru(0001). In *Desorption Induced By Electronic Transitions, DIET V*; Springer Series in Surface Science; Springer: Berlin, 1993; Vol. 31, pp 182−188.
(68) Madey, T. E.; Sack, N. J.; Akbulut, M. *Nucl. Instrum. Methods Phys. Res. B* **1995**, *100*, 309.

(69) Nair, L.; Sack, N. J.; Madey, T. E. *Nucl. Instrum. Methods Phys. Res. B* **1995**, *101*, 79.
(70) MacNeil, K. A. G.; Thynne, J. C. J. *J. Phys. Chem.* **1970**, *74*, 2257.
(71) Akbulut, M.; Madey, T. E.; Parenteau, L.; Sanche, L. *J. Chem. Phys.* **1996**, *105*, 6032.
(72) Akbulut, M.; Madey, T. E.; Parenteau, L.; Sanche, L. *J. Chem. Phys.* **1996**, *105*, 6043.
(73) Huuheey, J. E. *Inorgic Chemistry*, 3rd ed.; Harper International: New York, 1983.
(74) Gorham, J.; Torres, J.; Wolfe, G.; D'Agostino, A.; Fairbrother, D. H. *J. Phys. Chem. B* **2005**, *109*, 20379.
(75) Current, J. H.; Burdett, J. K.; Hodges, L.; Dunning, V. *J. Phys. Chem.* **1970**, *23*, 4053.
(76) Lugez, C. L.; Irikura, K. K.; Jacox, M. E. *J. Chem. Phys.* **1998**, *108*, 8381.
(77) Thurier, C.; Doppelt, P. *Coord. Chem. Rev.* **2008**, *252*, 155.
(78) Furuya, K.; Takeguchi, M.; Song, M.; Mitsuishi, K.; Tanaka, M. *J. Phys.: Conf. Ser.* **2008**, *126*, 012024.
(79) Guan, Y.; Fowlkes, J. D.; Retterer, S. T.; Simpson, M. L.; Rack, P. D. *Nanotechnology* **2008**, *19*, 505302/1.
(80) Klein, K. L.; Randolph, S. J.; Fowlkes, J. D.; Allard, L. F.; Meyer, H. M., III; Simpson, M. L.; Rack, P. D. *Nanotechnology* **2008**, *19*, 345705/1.
(81) Gabureac, M.; Bernau, L.; Utke, I.; Boero, G. *Nanotechnology* **2010**, *21*, 115503.